Supplemental Figures

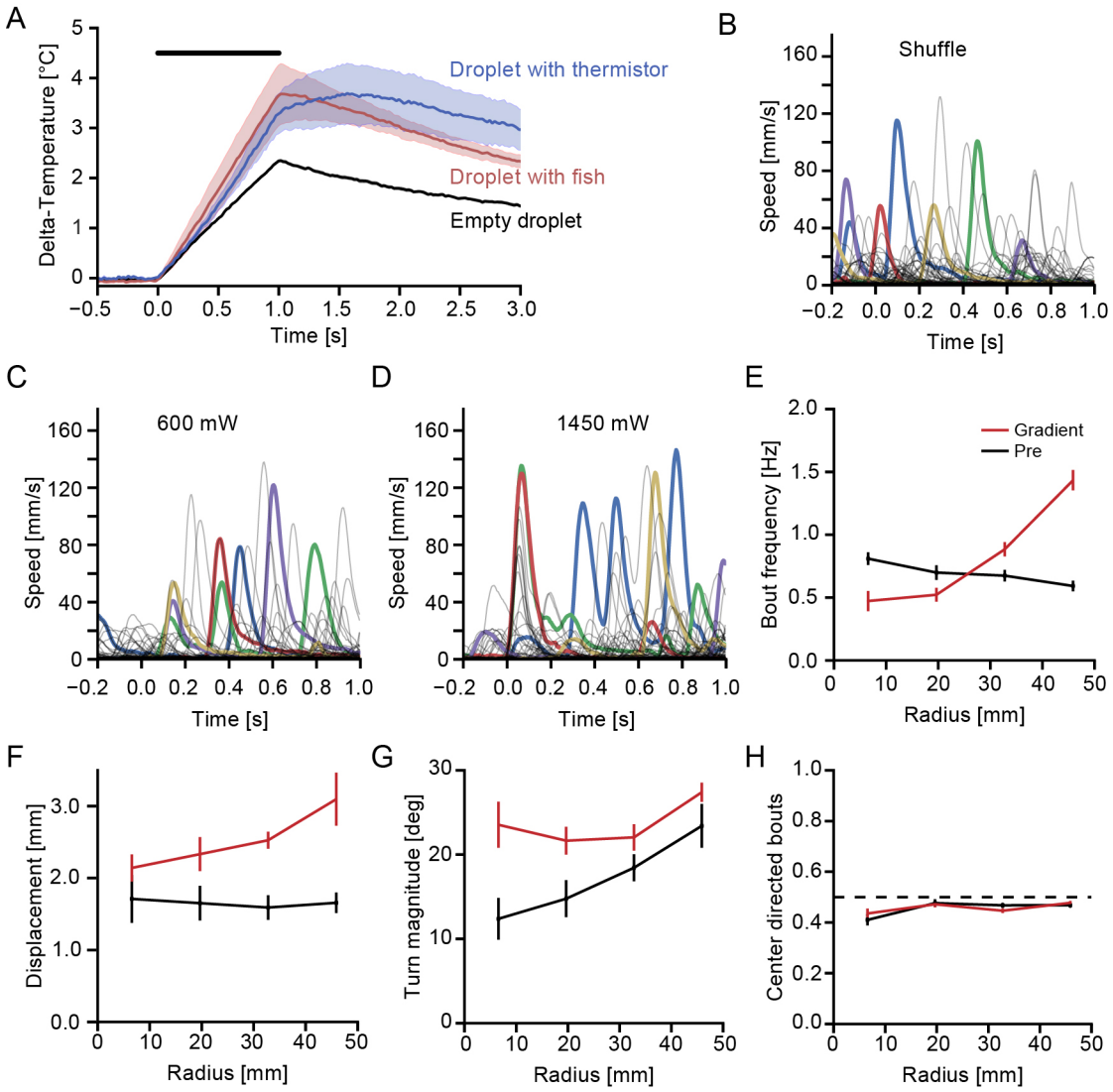

Figure S1. Related to Figure 1. The laser heating setup and behavioral characterization.

(**A**) Comparison of heating kinetics of small agarose droplets that are either empty (black trace), contain a larval zebrafish (red trace) or the thermistor used for establishing the heating model (blue trace) in response to a 1 s pulse (thick black bar) of 1450 mW laser power. Temperature measurements were done using a thermal imager. The considerably faster and larger rise in droplets that contain either a pigmented fish or a thermistor indicates that both are heated by direct absorption of laser power while the proximity of the traces suggests that absorption is similar for pigmented fish and the thermistor. The larger noise in the measurements of non-empty droplets is likely caused by the difficulty of controlling embedding depth and precise targeting of the laser using the thermal imager. Shaded area is standard error of the mean.
N = 8 for empty droplets and droplets with larval zebrafish, N = 3 for droplets with thermistor.
(**B-D**) Each plot depicts 100 randomly selected instantaneous speed traces around random time-points (B),

around the time of delivering a 600 mW power step (C) or a 1450 mW power step (D). In each plot 5 representative traces are highlighted by color to visualize progression of individual trials.
(**E-H**) Fish-averaged bout parameters according to binned radial gradient position during the virtual radial gradient experiments. Black, pre-gradient period, red gradient period. Error-bars indicate bootstrap standard error (N = 25 fish).
(**E**) Bout frequency at indicated radial positions.
(**F**) Per-bout displacement at indicated radial positions.
(**G**) Turn magnitude at indicated radial positions. The steady increase during pre-gradient conditions may underly thigmotaxis.
(**H**) At each position the fraction of bouts that were directed towards the center was evaluated. If the fish would navigate the gradient using a global strategy, it would be expected that the fraction of center-directed bouts would increase during gradient compared to pre-gradient conditions. The result therefore indicates that fish follow a strategy of local decisions to navigate away from the edge of the dish.

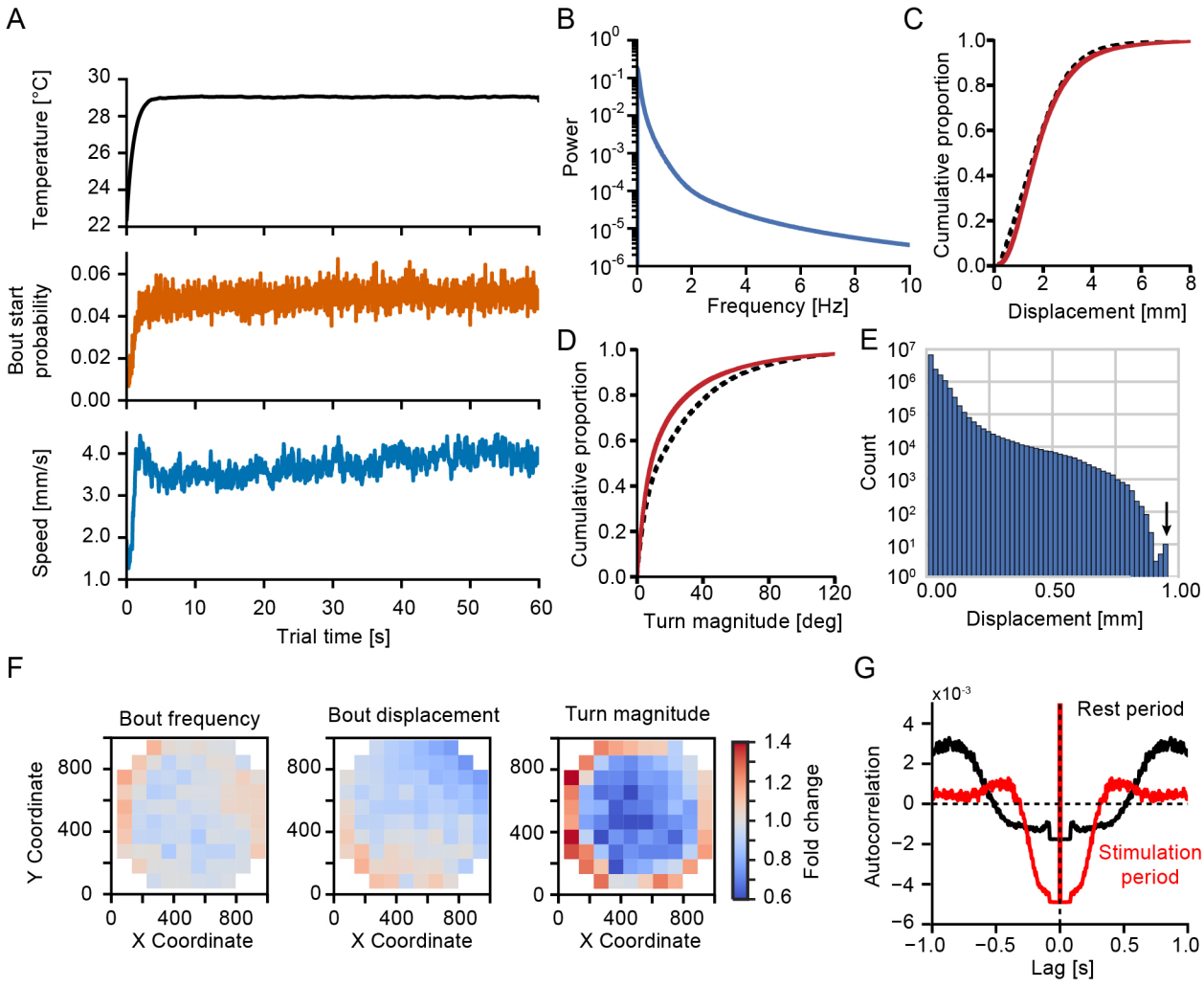

Figure S2. Related to Figure 2. The white noise heating paradigm.

(**A**) Average development of temperature and behavioral parameters during white-noise stimulation trials. Each plot is an average across 2200 stimulation trials of 50 fish. Top trace shows temperature average which is flat except for the initial rising phase on stimulus start. Orange middle trace shows average bout start probability in each 40 ms bin across trial time. Note that the initial rise in swim probability tracks the rise in temperature and that habituation across the length of the trial is minimal. The similar kinetics in the rise of predicted temperature and bout frequency argue for the correctness of the time-constant derived in the heating model. Blue bottom trace shows average swim-speed, which rises with similar kinetics as the heat stimulus and shows little, if any, habituation.

(**B**) Frequency spectrum of the white noise stimulus.

(**C**) Cumulative distribution of bout displacements across all white-noise experiments. The dashed black line is the cumulative distribution during resting while the solid red line depicts the cumulative distribution during laser stimulation.

(**D**) Same as in (C) but for bout turn magnitudes. The rightward shift of the cumulative distribution indicates that the white noise stimulus suppresses turning.

(**E**) Histogram of per-frame (4 ms interval) displacements during swims across all fish and stimulation trials. Displacements of routine bouts form a continuous distribution but note the second peak (indicated by arrow) which marks large magnitude escapes. These occur with a probability of less than 1% during stimulation trials.
(**F**) Influence of arena position on bout parameters. For each fish, position was binned into the squares shown. For each bin the average of the given parameter was divided by the fish-median and the resulting maps were averaged across fish. Each plot depicts the average deviation from the median of the indicated swim parameter across fish. Note that modulation is small except for a large increase in turn magnitude at the edge of the dish. Frames in which the fish was close to the edge of the arena were excluded from model derivations.
(**G**) Autocorrelations of bout starts across all experiments for resting (black line) and stimulation (red line) periods. Both during resting and during stimulation there is a clear refractory period. The difference between the two lines likely indicates the influence of the stimulus on bout generation (such as a shortening of inter-bout-intervals, Figure 2D). The 80 ms long flat line around zero time lag is due to a minimum 80 ms bout duration enforced by the bout detection algorithm.

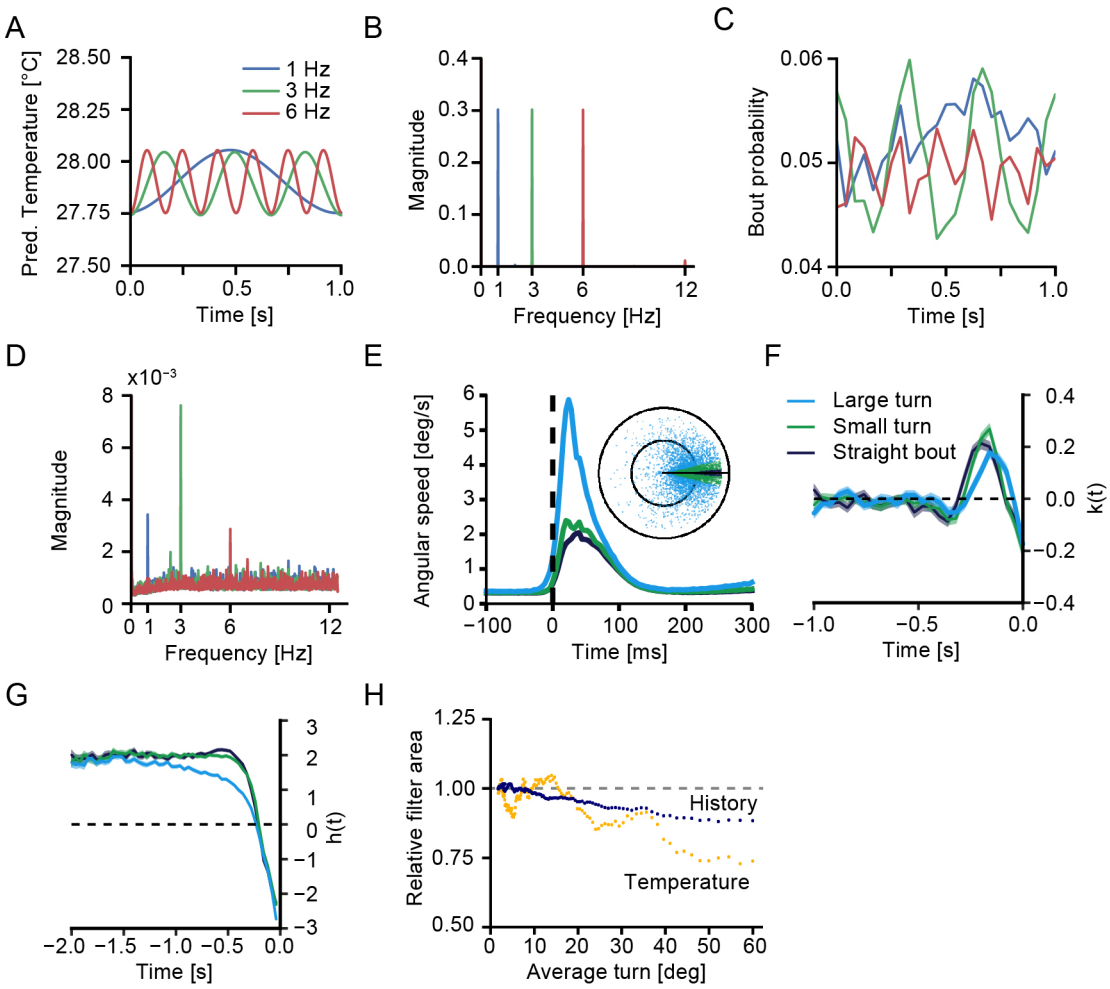

Figure S3. Related to Figure 3. Generalized linear models of bout initiation.

(**A**) Stimuli for 1 Hz (blue), 3 Hz (green) and 6 Hz (red) stimulation periods. Temperatures shown are predictions based on the heating model. The traces depict one second of each stimulus. Note that all stimuli are matched in temperature amplitude and average according to the heating model.
(**B**) Fourier transform of 1 Hz (blue), 3 Hz (green) and 6 Hz (red) temperature stimuli revealing the similarity in magnitudes for each stimulus at its stimulation frequency.
(**C**) Average bout initiation probability across all fish during 1 Hz (blue), 3 Hz (green) and 6 Hz (red) stimulation periods. The first 10 seconds of each trial have been excluded as they contain an initial temperature rise (similar to Figure S1A). Bout probabilities have been computed by averaging bout starts in each 40 ms timebin across all individual 1 s stretches of all fish and all trials of the same stimulation frequency. This was done to reduce noise for display purposes.
(**D**) Fourier transform of response probabilities during 1 Hz (blue), 3 Hz (green) and 6 Hz (red) stimulation periods. The Fourier transform was computed after determining response probabilities across all fish and all trials. The first 10 seconds of each trial were excluded and probabilities were calculated across a total of 450 trials per frequency from 50 fish.
(**E-G**) GLMs for bouts of different turn magnitude (N=28577 bouts in each group). Shaded areas indicate

bootstrap standard error.
(**E**) Average angular speed profiles during “Straight”, “Small turn” and “Large turn” bouts. Inset depicts the endpoints of the different bout categories if the fish were facing left (black circles delineate 2 and 4 mm of displacement).
(**F**) Coefficients of the temperature responsive part $k(t)$ of turn category GLMs versus time before bout onset.
(**G**) Coefficients of the bout history responsive part $h(t)$ of turn category GLMs versus time before bout onset.
(**H**) Relative area of temperature (orange) and bout-history (blue) filter for groups of 25000 bouts with the indicated average turn magnitude. Dashed grey line indicates area of group with lowest turn magnitude.

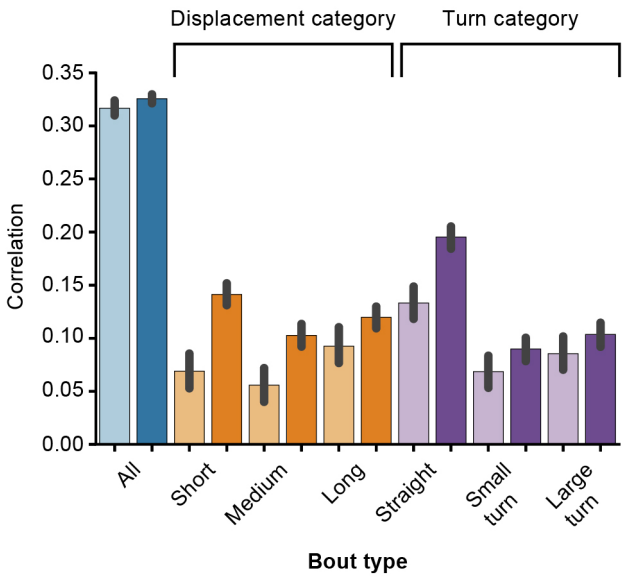

Figure S4. Related to Figure 4. Single fish variability and prediction.

For each indicated bout category (all bouts blue, displacement categories orange, turn categories violet) the figure depicts the average correlation of bout probabilities across time during the playback period for each pair of fish in the light colored bars. Response probabilities per 40 ms time-bin were derived by averaging responses across 88 playback trials for each fish and convolving the resulting trace with a gaussian filter with a standard deviation of 2 time-bins (80 ms). The dark colored bars are a correlation between each individual fish response and model instantiation averages across 88 trials with the playback stimulus as model input (single fish predictions). Model averages were convolved with the same gaussian filter.
Error bars are bootstrap 95% confidence intervals.

Supplemental Movies

Movie S1, related to Figure 1. Swim response to a 1450 mW power step. The video shows an example response of a larval zebrafish to a 2 s long power step of 1450 mW power at sample. The left panel shows the behavior with the fish's centroid used for tracking marked with a black asterisk during rest while the laser beam (to scale) is indicated during stimulation. The right panel shows the instantaneous speed of the fish on the left visualizing the increase in swim frequency and vigor upon laser stimulation. The period of laser stimulation is indicated by the red line color. Video is slowed down ten-fold.

Supplemental tables

Table S1: Cross validations reveal model fidelity. Refers to Materials and Methods.

	Correlation	**Slope of fit**	**Area under ROC curve**
All bout model	1.00	1.01 ± 0.07	0.71 ± 0.01
Displacement categories			
Short bout model	1.00	1.04 ± 0.20	0.71 ± 0.01
Medium bout model	0.99	1.01 ± 0.11	0.73 ± 0.01
Long bout model	0.99	0.99 ± 0.15	0.72 ± 0.01
Turn categories			
Straight bout model	1.00	1.03 ± 0.11	0.73 ± 0.01
Small turn model	1.00	1.01 ± 0.10	0.72 ± 0.01
Large turn model	1.00	1.01 ± 0.13	0.73 ± 0.01

Refers to materials and methods. For each model the table depicts three parameters extracted during 250 cross-validations. The first column lists the correlation of predictions on the test-set versus actual observed bout counts binned by predicted probability. The predicted bout count is the number of times a given predicted probability bin is observed times the average probability within the bin, while the observed count is the number of bouts actually observed for a given probability bin. The second column lists the slope of a fit of bout count predictions versus actual observed bout counts. The third column indicates the area under the receiver-operator-curve when using the model as a classifier (bout versus inter-bout frame) on the test-set. Columns list the mean $\pm$ standard deviation of each metric except in the first column where the standard deviation was always smaller than 0.01.

Table S2: Constant terms of generalized linear models. Refers to Materials and Methods.

	b_0
All bout model	-3.6
Displacement categories	
Short bout model	-4.9
Medium bout model	-5.0
Long bout model	-4.9
Turn categories	
Straight bout model	-5.0
Small turn model	-4.9
Large turn model	-4.8

For each model the table depicts the value of the constant term b_0.

Supplemental Materials and Methods

Behavioral apparatus

Setup While fish were freely exploring their arena we acquired images at 250 Hz using a Gazelle GZL-CL-22C5M-C camera (Point Grey Research, Inc., Canada) utilizing a NI PCIe-1433 frame grabber (National Instruments Corporation, USA). The arena was illuminated from below using 880 nm IR LEDs. Visible light and reflections of the laser were blocked using a 880 nm bandpass filter (Thorlabs, USA). Custom written software in C# (Microsoft, USA) extracted the fish position and heading angle in realtime (average time from image acquisition to position: 0.3 ms). The position information was used to send voltage commands via an NI PCIe-6343 DAQ board (National Instruments Corporation, USA) to a set of 6210H Galvos rotating 3 mm diameter X/Y scan mirrors (Cambridge Technology, USA). Our software performed a two-step calibration routine, first roughly aligning pixel coordinates and angles by triangulation followed by the generation of a 10 pixel spaced lookup table. This resulted in an average targeting accuracy of the center of the laser beam to within less than one pixel ($\approx 111\,\mu\mathrm{m}$) deviation from the intended location. The mirror commands were therefore calibrated such that the laser was centered on the centroid of the tracked fish object at all times. This was further verified by removing the blocking bandpass filter and visualizing brief laser pulses together with the tracked fish. During these tests we never observed mis-targeting of the laser beam. At the same time the output power of an SDL-980-LM-8000T (Shanghai Dream Lasers, China) infrared laser operating at 980 nm with a maximum output power of 8 W was controlled according to the specific behavioral paradigm by supplying appropriate voltage commands to the laser current driver. The laser beam was slightly focused using a 750 mm focal length lens (Thorlabs, USA) to a spot diameter of 5 mm at sample, measured using an IR fluorescent alignment disc (Thorlabs, USA). This size is slightly larger than the length of a larval zebrafish at this age ($\sim 4\,\mathrm{mm}$, see inset in Figure 1A, Main text). The relationship between laser output power and power at sample was determined over the full power range using a PM100D optical power meter with a S310C sensor (Thorlabs, USA).

Temperature calibration To correspond delivered laser power with temperature and to determine the temporal kinetics of heating a 4 mm long, 840 μm diameter, thermistor was used (Warner Instruments,

USA) to measure temperature changes in the water in response to laser power steps of different magnitude (Figure 1B-C, Main text). In order to relate input power $I(t)$ to temperature $U(t)$ two parameters were estimated, the heating rate α and the Newtonian cooling rate β. After subtracting the resting temperature T_0 the change in temperature can be described by the following differential equation:

$$\frac{dU}{dt} = \alpha\, I(t) - \beta U \tag{S1}$$

β was estimated by an exponential fit to the cooling phase after laser-offset ($\rightarrow I(t) = 0$) according to:

$$U = U_{max} e^{-\beta t} \tag{S2}$$

β was found to be $0.98\,\mathrm{s}^{-1}$ corresponding to a half-time of 700 ms and α was subsequently estimated during constant laser input ($\rightarrow I(t) = I$) by substitution into (S1):

$$\alpha = \frac{\delta U + \delta t \beta U}{\delta t I} \tag{S3}$$

The estimation for α was $8.80\,^{\circ}\mathrm{C}/\mathrm{J}$. Parameter fitting allowed conversion of our laser input sequence to a temperature estimate by evolving

$$U(t+\delta t) = U(t) + \delta t\big(\,\alpha\, I(t+\delta t) - \beta\, U(t)\,\big) \tag{S4}$$

at discrete time steps of length δt.

Thermal imager measurements A GOBI XC208 thermal imager (Xenics, Belgium) was used to test whether pigmented larval zebrafish and the thermistor used for calibration are likely heated directly by the laser or via heating of the surrounding water. Unfortunately the imager could not be used to directly derive our heating model as the wavelength detected by the imager ($8 - 14\,\mu\mathrm{m}$) is nearly completely absorbed by water making it impossible to directly detect the temperature of a submerged object. The imager was therefore used to gain indirect evidence for direct absorption of a pigmented zebrafish larva as well as our thermistor by their influence on the heating of small droplets of agarose. To this end the heating profiles in response to a 1 s long laser pulse at 1450 mW were compared between empty droplets, droplets containing an embedded larval zebrafish as well as droplets containing an embedded thermistor head. Larval zebrafish were anesthetized using MS-222 before embedding. For conversion of intensity levels reported by the thermal imager to temperature values, the imager was calibrated by filming water heated to different temperatures.

Behavioral protocols

Power steps To determine behavioral response time to changes in laser power, fish were presented with laser power steps. The paradigm consisted of 45 presentations each of 2 s long steps of 600 mW and

1450 mW laser power at sample in random order, corresponding to a temperature increase on the order of 5 °C and 13 °C respectively. Stimuli were interleaved with 18 s of resting time.

Radial gradient To test heat avoidance in our setup zebrafish were exposed to a virtual radial gradient of laser power where power delivered to the fish was set based on radial position. Experiments consisted of a 30 minutes long pre-gradient time followed by 30 minutes of a quadratically rising gradient with 0 mW power at the dish center up to 1084 mW at sample at the dish edge, Figure 1E (corresponding to $\sim$22 °C in the center and $\sim$32 °C at the edge). A quadratic function was chosen for the gradient to create a spatially uniform distribution of power levels within the circular arena.

Frequency stimulation For frequency stimulation fish were presented with sinusoidal temperature stimuli at 1 Hz, 3 Hz and 6 Hz (Figure S3A). Laser power amplitudes of the stimuli were derived empirically such that the heating model predicts the same amplitude for all stimuli (see below). Each fish was presented in random order with 9 one-minute-long repetitions of each stimulation frequency followed by 1 minute resting. The laser power amplitudes used during frequency stimulation experiments were 140 mW for the 1 Hz stimulus, 438 mW for the 3 Hz stimulus and 897 mW for the 6 Hz stimulus. After low-pass filtering of the heating model all these stimuli were predicted to result in a temperature amplitude of 0.15 °C.

Data analysis

Fish position and heading angle were extracted online at 250 Hz using custom software written in C# (Microsoft). The obtained behavioral data was further analyzed using custom software written in Python (python.org, version 3.4) using NumPy (van der Walt $\mathrm{et\ al.}$, 2011), SciPy (Jones $\mathrm{et\ al.}$, 2007) and Scikit-learn (Pedregosa $\mathrm{et\ al.}$, 2011). Plots were generated using Matplotlib (Hunter, 2007) and *Seaborn*.
All fish that completed all trials were included in the analysis. Occasionally fish would stop moving during the assay or would not move at normal frequency during the habituation phase which preceded every experiment. These experiments were stopped and not used for analysis.

Behavioral parameters The instantaneous speed of fish in each frame was extracted from a filtered version of the position trace (biphasic filtering, window size 11 frames) and used to identify individual swim-bouts. Swim-bouts were identified based on threshold crossing of the instantaneous speed (2 $^{\mathrm{mm}}/_{\mathrm{s}}$) for at least 80 ms and were required to have a clearly defined peak (shorter than 20 ms) in the instantaneous speed trace. These criteria were derived manually, comparing visually identified bouts in the trace to automated bout detection. This simple algorithm allowed us to identify swim-bouts with an accuracy $> 99\%$. For all following analysis the behavioral data and temperature traces were binned 10-fold to a final framerate of 25 Hz. For each bout the distance moved was computed with respect to the bout-starting point. At the same time the angular displacement was determined with respect to the starting axis of each bout. These metrics were used to subdivide different bout-types based on distance traveled or turn angle.

Model fitting The filter kernels $\vec{k}$ and $\vec{h}$ were estimated via maximum likelihood using Scikit-learn's interface to LIBLINEAR (Fan $\mathrm{et\ al.}$, 2008). Because of the fairly large auto-correlation in our stimulus (Figure 2C) $L2$ norm regularization was employed in our fit to dampen noisy fluctuations as in ridge regression (Hastie

$\mathrm{et\ al.}$, 2001). LIBLINEAR fits $b = \{b_0; \vec{k}; \vec{h}\}$ by minimizing the sum of a regularization term and the negative log-likelihood of the logistic model:

$$\underset{b}{min} \qquad \frac{1}{2} b^T b + C \sum_{i=1}^{N} log\left(1 + e^{-y_i b^T x_i}\right) \quad | \, y_i = \begin{cases} +1 & \text{at bout start} \\ -1 & \text{everywhere else} \end{cases} \tag{S5}$$

The regularization term was set to $C = 0.01$, in our case resulting in a mild regularization of the regression. Models were fitted for the occurrence of any bout as well as bouts corresponding to a specific distance or turn category. Distance and turn categories were determined by subdividing the observed, more or less continuous bout distance and turn angle distributions. Our independent variable $y(t)$ was set to 1 for each bin in which a bout of the given category occurred. Our bout-history term, $\vec{n(t)}$, always took all bouts into account regardless of their category since we expect that the time of the last swim event rather than its type has the largest influence on bout initiation.
Since the edge of the behavioral arena might influence the turn magnitude or displacement of a bout independent of thermal input (Figure S2F), all timepoints in which the fish was closer than 5 mm to the wall of the chamber were excluded from the computation of our category bout models (this removed 59% of all bouts from the analysis). Such timepoints were also excluded from the corresponding validations below. Displacement category bouts were restricted to a maximum turn magnitude of 40 degrees (84% of bouts) and turn category bouts were restricted to a maximum displacement of 3.6 mm (88% of bouts). This was done to minimize influences of displacement variation on turn magnitude and vice versa.
Standard errors and confidence intervals of the fits were estimated by bootstrapping the regression models (Efron and Tibshirani, 1993; Fox, 2008).

Model validation The time rescaling theorem (Brown $\mathrm{et\ al.}$, 2002) was employed as follows to test how accurately our general bout model can predict bout latencies. To this end the original bout times $n = t(bout_i)$ were transformed per the equation

$$N = \sum_{t=0}^{t=n} p(bout \mid t) \tag{S6}$$

using equations (1, 2, Main text) and the transformed bout latencies L were calculated as

$$L_i = N_i - N_{i-1} \tag{S7}$$

L is expected to follow an exponential distribution with $\lambda = 1$ and therefore after the transformation

$$z_i = 1 - e^{-L_i} \tag{S8}$$

z_i are expected to be uniformly distributed random variables on the interval $[0, 1)$.

Model sensitivity Our models are composed of the temperature filter and the history filter. We reasoned that the area of these filters, i.e. the absolute sum of the coefficients, indicates how sensitive the model is

to changes in each of these components. To determine how the sensitivity of the two filters changes with changes in bout parameters all observed bouts were ordered by their displacement (or turn magnitude) and bins of 25,000 bouts (25% of all non-edge bouts) with varying average displacement (turn magnitude) were created. Models were subsequently fit using bouts within each bin as our behavioral output and the filter areas in each bin were computed.

Frequency response experiments To compute the response magnitude at each frequency all trials with the same stimulation frequency of all fish were used to compute the average response probability in each 40 ms time-bin. The first 10 seconds of each trial were excluded from this analysis since this is the time needed for the average temperature to fully reach equilibrium. Subsequently the Fourier transform was computed on these probability traces (Figure S2D) and the response magnitude at each frequency was extracted. To test for significant differences in response magnitudes at the principal frequencies (1 Hz for the 1 Hz stimulus, etc.) a bootstrap hypothesis test was used. Since the computation of response probabilities requires an average across trials and individual fish averages were too noisy we effectively computed p-values for the differences of the sums of all principal frequencies across different stimulation types. We note that this approach likely underestimates the real differences somewhat as, e.g., 6 Hz responses during 1 Hz stimulation are mostly due to noise.

Supplemental References

Brown, E., Barbieri, R., Ventura, V., Kass, R. and Frank, L. (2002). The Time-Rescaling Theorem and Its Application to Neural Spike Train Data Analysis. Neural Computation *14*, 325–346.

Efron, B. and Tibshirani, R. (1993). An Introduction to the Bootstrap. CRC Press.

Fan, R.-E., Chang, K.-W., Hsieh, C.-J., Wang, X.-R. and Lin, C.-J. (2008). LIBLINEAR: A Library for Large Linear Classification. The Journal of Machine Learning Research *9*, 1871–1874.

Fox, J. (2008). Applied Regression Analysis and Generalized Linear Models. SAGE Publications.

Hastie, T., Tibshirani, R. and Friedman, J. (2001). The elements of statistical Learning Springer. New York.

Hunter, J. D. (2007). Matplotlib: A 2D Graphics Environment. Computing in Science & Engineering *9*, 90–95.

Jones, E., Oliphant, T. and Peterson, P. (2007). SciPy: Open source scientific tools for Python, 2001–. URL http://www.scipy.org.

Pedregosa, F., Varoquaux, G., Gramfort, A., Michel, V., Thirion, B., Grisel, O., Blondel, M., Prettenhofer, P., Weiss, R., Dubourg, V., Vanderplas, J., Passos, A., Cournapeau, D., Brucher, M., Perrot, M. and Duchesnay, É. (2011). Scikit-learn: Machine Learning in Python. The Journal of Machine Learning Research *12*, 2825–2830.

van der Walt, S., Colbert, S. C. and Varoquaux, G. (2011). The NumPy Array: A Structure for Efficient Numerical Computation. Computing in Science & Engineering *13*, 22–30.